

Artigo

Radiation Balance Estimates Over Southeastern Brazil: Ground Observations, Satellite and Reanalysis

Cristian Felipe Zuluaga^{1,2} , Flavio Barbosa Justino¹ , Almir Venancio Ferreira³,
Jose Marinaldo Gleriani⁴ 

¹*Departamento de Engenharia Agrícola, Universidade Federal de Viçosa, Viçosa, MG, Brazil.*

²*Facultad de Ciencias Agrarias, Corporación Universitaria Santa Rosa de Cabal, Santa Rosa de Cabal, Colombia.*

³*Centro Federal de Educação Tecnológica Celso Suckow de Fonseca, Rio de Janeiro, RJ, Brazil.*

⁴*Departamento de Engenharia Florestal, Universidade Federal de Viçosa, Viçosa, MG, Brazil.*

Recebido em: 17 de Fevereiro de 2022 - Aceito em: 4 de Fevereiro de 2023

Resumo

Pela grande atividade econômica e densidade populacional, a região sudeste do Brasil vivencia processos acelerados de mudanças no uso e cobertura do solo, que contribuem para modificações no balanço de radiação (BR) na superfície. Neste estudo, avaliamos os componentes do BR de diferentes conjuntos de dados de alta resolução, última geração, nesta região do país em dois períodos (fev/2005-jan/2006 e mar/2015-fev/2016). Em geral, todos os conjuntos de dados representaram adequadamente a sazonalidade dos componentes do BR (exceto albedo). O ERA5-Land apresenta com o menor erro relativo médio para representar o albedo ($\approx 15\%$), radiação de onda longa atmosférica ($DLWR \approx 4,5\%$) e radiação de onda longa da superfície ($ULWR \approx 3,6\%$). Na estimativa de radiação de ondas curtas, o GLASS foi o melhor ($\approx 14\%$). As incertezas neste último podem estar associadas à dificuldade para representar a variabilidade de cobertura de nuvens no período chuvoso. As falhas na estimativa do albedo devem-se à incapacidade de simular as propriedades da superfície. $DLWR$ e $ULWR$ apresentaram os melhores desempenhos e suas incertezas estiveram relacionadas a problemas no cálculo das temperaturas do ar e da superfície, respectivamente. ERA5-Land e GLASS são adequados para estimar os componentes da BR no sudeste do Brasil.

Palavras-chave: ERA5-Land, GLASS, GLDAS, Sudeste do Brasil, balanço de radiação.

Estimativas do Balanço de Radiação no Sudeste do Brasil: Observações, Satélite e Reanálise

Abstract

Due to the high economic activity and population density, the southeast region of Brazil experiences accelerated processes of changes in land use and cover, which contribute to modifications in the radiation balance (RB) at the surface. In this study, we evaluated the RB components from different state-of-the-art high resolutions datasets over this region of the country during two periods (Feb/2005-Jan/2006 and Mar/2015-Feb/2016). In general, all datasets adequately represented the seasonality of the RB components (except albedo). The ERA5-Land has the lowest mean relative error to represent albedo ($\approx 15\%$), downwelling longwave radiation ($DLWR \approx 4.5\%$) and upwelling longwave radiation ($ULWR \approx 3.6\%$). In the case of the downwelling shortwave radiation estimation, GLASS was the best ($\approx 14\%$). Uncertainties in the latter may be associated with the difficulty in representing the variability of cloud cover during the rainy season. Failures in estimating albedo are due to the inability to simulate surface properties. $DLWR$ and $ULWR$ presented the best performances and their uncertainties were related to problems in the computation of air and surface temperatures, respectively. ERA5-Land and GLASS are adequate to estimate RB components in southeastern Brazil.

Keywords: ERA5-Land, GLASS, GLDAS, Southeast Brazil, radiation balance.

1. Introduction

Brazilian southeast region (SE) is the main driver of economic development in the country, since it concentrates around 42% of the population and produces approximately 56% of the gross domestic product (IBGE, 2018). All this development lead to large changes in land cover. Urban areas, pastures and crops - such as coffee, soy and sugarcane - replaced areas of native vegetation in the Atlantic Forest and Cerrado biomes, leaving them with a low proportion of remaining native vegetation and biodiversity highly threatened (Alvarenga *et al.*, 2016; Dias *et al.*, 2016; Grecchi *et al.*, 2014; Sano *et al.*, 2010).

Microclimate studies of biomes associate deforestation with potential impacts on the climate system, primary caused by changing the components of radiation balance (RB) (Conte *et al.*, 2019; Macdougall and Beltrami, 2017). Estimates of the amount of solar energy received, reflected and emitted by the Earth's surface and the atmosphere, plays a prominent role to the understanding of past weather, long-term features and future climate (Wild, 2016, 2020). Moreover, the study of the radiation balance on the earth's surface is relevant to solve some scientific questions, such as the practical viability of solar energy, the reaction of plants to the wavelengths necessary for photosynthesis, the potential consumption of water and productivity of crops/ecosystems, among others. (Green *et al.*, 2017; Mercado *et al.*, 2009; Wild *et al.*, 2015).

Observations of the RB components have been carried out for some decades through net radiometers (Driemel *et al.*, 2018; Wild *et al.*, 2017). However, this instrumentation besides having a high cost and requiring special techniques of operation and calibration, provides measurements that are representative only for small areas that cannot be used at larger scales (Ferreira *et al.*, 2020). In most case in Brazil meteorological stations only measures shortwave component (Xavier *et al.*, 2016), while the longwave component is restricted to individual micro-meteorological experiments or recent networks of specialized stations, such as SONDA (INPE, 2021).

Remote sensing and reanalysis appear as alternatives to solve the absence and limitations of surface measurements of the RB components. There are two types of remote sensing algorithms, those that use only information from satellite sensors (Bisht *et al.*, 2005; Ramirez-Cuesta *et al.*, 2018), and others that combine on-board sensors with surface station data (Amatya *et al.*, 2015; Carmona *et al.*, 2015; Ferreira *et al.*, 2020; Silva *et al.*, 2015). However, previous methodologies has been restricted to cloudless days. Bisht and Bras (2010, 2011) proposed a model to estimate the RB components (instantaneous and daily) for all sky conditions, which uses only MODIS sensor information. Although useful, this methodology computed the daily RB from only two measurements, which are insufficient to capture cloud dynamics, especially for

latitudes higher than 30°, where the MODIS's passage is 1-2 days (Wolfe *et al.*, 2002). On the other hand, reanalyses offer temporal high resolution and consistency, as well as data under all sky conditions. These are frequently used for atmospheric model validation, and have contributed to clarify the relative importance of the data assimilation improvements versus observational improvements for numerical weather prediction over the last decades (Bengtsson *et al.*, 2007). However, caveats result from their coarse resolutions (> 100 km) and assimilation of data obtained from atmospheric profiles and measurements, which cause systematic biases in the RB products (Jia *et al.*, 2018; Slater, 2016; Zhang *et al.*, 2016).

To overcome the problems mentioned above, studies have combined satellite and reanalysis data to determine the RB components at global (Verma *et al.*, 2016) and regional scales (Moukomla and Blanken, 2017; Oliveira *et al.*, 2016; Yu *et al.*, 2014). In addition, with the recent advances in data assimilation, increment in the quality and quantity of observed data, increase in spatial resolutions (< 30 km) and improvements in the parameterization of models, blended datasets have been made available for involving different meteorological parameters, such as the RB components (Muñoz-Sabater *et al.*, 2021; Rodell *et al.*, 2004; Zhang *et al.*, 2019). Nevertheless, it is crucial to assess the reliability of each dataset, and to identify the strengths and underlying biases associated, before using them (Dolinar *et al.*, 2016).

In this context, the present study focuses on evaluating the performance of state-of-the-art high-resolution datasets (reanalyses and satellite), that can suitably fill the lack of observation in Brazil as an alternative for monitoring the RB components. The paper is structured as follows. Section 2 introduces the study area, climate datasets and methods. Section 3 details and discusses the performance in estimating the RB components based on different datasets, while the section 4 presents the concluding remarks.

2. Materials and Methods

2.1. Study area

The study area corresponds to the southeast region of Brazil, located between latitudes 14° S and 25° S and longitudes 54° W and 39° W (Fig. 1). The region has a territorial extension of 924,620 km² (approximately 10 times the Portugal surface area, or 1.6 times of the Iberian Peninsula), formed by the States of Minas Gerais (MG), São Paulo (SP), Espírito Santo (ES) and Rio de Janeiro (RJ). In addition, it has a population of approximately 88.6 million people. The region is covered by Mata Atlântica (Atlantic Forest), Cerrado (Savanna) and Caatinga (Fig. 1b). Mata Atlântica is concentrated mainly in the east of the territory, while Cerrado is present in the interior of

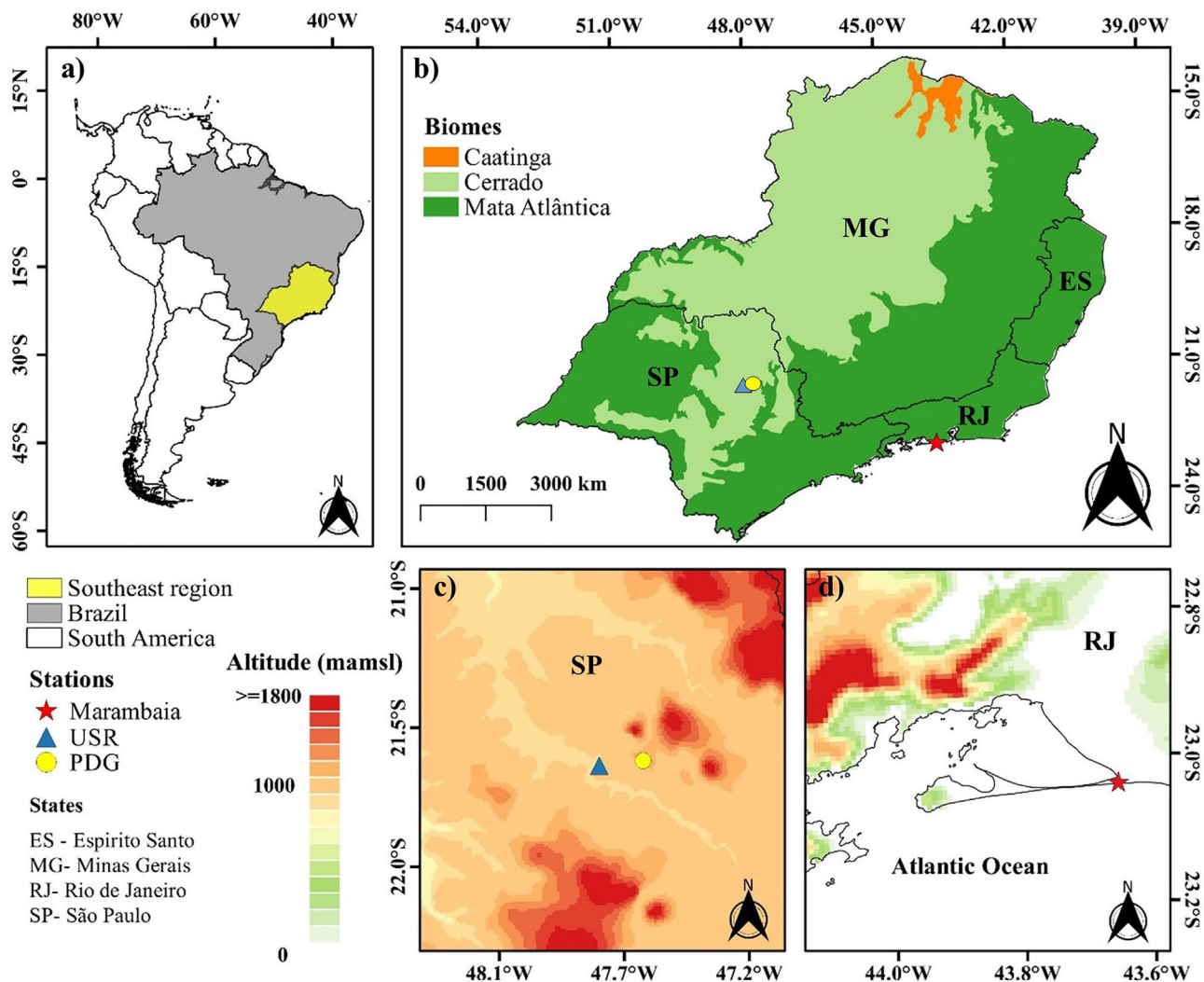


Figure 1 - Study area characteristics and localization of stations.

SP and west of MG. Caatinga biome corresponds to small portion of the north of the region. The seasonal cycle of precipitation, humidity and circulation are determined by the South Atlantic Convergence Zone (SACZ) during the spring and summer seasons, while the frontal systems dominate the winter season, which is predominantly dry (Bernardino *et al.*, 2018; Zilli *et al.*, 2017). The relief, which varies from sea level to altitudes above 1800 m, has an influence on the region temperature, decreasing it as the elevation increases (Cavalcanti *et al.*, 2009).

2.2. Observed data for validation

Measurements of the RB components from three different surfaces were used to validate the dataset outputs, as described below. These stations are representative of three different environment conditions, in terms of vegetation and land cover changes. The short data collection periods (one year) are because the all stations were part of short-term academic projects.

2.2.1. USR station

This is an experimental sugarcane field belonging to Power Plant Santa Rita (USR) located in the State of SP (Fig. 1c). This station measures (latitude 21°38'13" S, longitude 47°47'25" W), downward shortwave radiation (*DSWR*), albedo (α), downward longwave radiation (*DLWR*) and upward longwave radiation (*ULWR*) that were collected between February-2005 and January-2006. This place has an average altitude of 552 m and corresponds to sugarcane plants in the first cycle of regrowth (Oliveira *et al.*, 2018; Silva *et al.*, 2015).

2.2.2. PDG station

This station is installed in the reserve Pé-de-Gigante (PDG) within the Vassununga State Park (Instituto Florestal) located in the State of SP (Fig. 1c). The station (latitude 21°37'9.26" S, longitude 47°37'56.38" W) measured *DSWR* and α between February-2005 and January-2006 as

well. This place corresponds to an area of 1,213 hectares of undisturbed woody savanna vegetation called Gleba Cerrado Pé-de-Gigante, with an average altitude of 710 m (Oliveira *et al.*, 2018; Silva *et al.*, 2015).

2.2.3. Marambaia station

Located in the permanent preservation area at Barra de Guaratiba, State of RJ (Fig. 1d), at latitude 23°03'1" S and longitude 43°35'34" W. The vegetation corresponds mainly to *Tapirira guianensis* Aubl and *Calophyllum brasiliensis* Cambess, and the soil, although with a sandy texture, presents a large amount of organic matter in the superficial horizons (Carvalho *et al.*, 2015; Pereira *et al.*, 2012). Here, *DSWR*, α , *DLWR* and *ULWR* were measured between March-2015 and February-2016.

2.3. Gridded datasets

Five different modern gridded datasets were used. The RB components were extracted directly from ERA5-Land, GLDAS and GLASS. Air temperature (*Ta*), *DSWR*, and incident solar radiation at the top of the atmosphere (*Ro*), used to compute *DLWR* with the SEBAL algorithm (Section 2.4), were extracted from the Xavier and CERES-SYN datasets. Table 1 summarizes the characteristics of each dataset.

ERA5-Land is based on running the land component from ERA5 reanalysis of the European Centre for Medium-Range Weather Forecasts (ECMWF) but without coupling to the atmospheric models (Cao *et al.*, 2020). This product has a spatial resolution of $0.1^\circ \times 0.1^\circ$, with hourly temporal frequency, from 1981 to present (Pelosi *et al.*, 2020). The radiation scheme performs calculations of the shortwave and longwave radiative fluxes using the predicted values of temperature, humidity, cloud, and monthly-mean climatologies for aerosols and the main trace gases (Muñoz-Sabater *et al.*, 2021).

The Global Land Data Assimilation System (GLDAS) reanalysis is a project lead by the National Aeronautics and Space Administration (NASA). The RB components are available in a spatial resolution of $0.25^\circ \times 0.25^\circ$, temporal resolution of 3 hours, for the 2000-present period (Oliveira *et al.*, 2016). The radiation fluxes are calculated as a function of atmospheric transmissivity and emissivity, which are determined by cloud type and amount, derived from NOAA satellites (Rodell *et al.*, 2004).

The Global Land Surface Satellite (GLASS) products are produced from multiple satellite observations, exploring the use of multiple algorithms for the same product to improve accuracy and stability, optimizing the use of temporal signatures in remote sensing data and the existing satellite high-level products (Liang *et al.*, 2013; Zhao *et al.*, 2013). Albedo and *DSWR* products are available in frequency of 8 days and 1 day, respectively. Both products have spatial resolution of $0.05^\circ \times 0.05^\circ$. The GLASS albedo product is produced from MODIS data, based on two direct estimation algorithms from surface reflectance, top of atmosphere radiance, and a statistics-based temporal filtering fusion algorithm (Liang *et al.*, 2013). The *DSWR* product of GLASS is generated based on an improved look-up table method using both polar-orbiting and geostationary satellite data, including MODIS, Meteosat Second Generation (MSG) SEVIRI, the Multi-functional Transport Satellite (MTSAT)-1R, and the Geostationary Operational Environmental Satellite (GOES) Imager (Zhang *et al.*, 2019, 2014).

Clouds and the Earth's Radiant Energy System (CERES) is a mission of NASA that provided the climate community a 20-yr record of observed top-of-the-atmosphere (TOA) fluxes (Doelling *et al.*, 2016). The CERES synoptic (SYN) product incorporates derived fluxes from the geostationary satellites (GEOs) in $1^\circ \times 1^\circ$ spatial resolution and daily temporal frequency. OBS-Brazil dataset

Table 1 - Characteristics of gridded datasets used in this study.

Data	Source	Resolution		Variables used	Available period
		Spatial	Temporal		
<i>Reanalysis</i>					
ERA5-Land	ECMWF	$0.1^\circ \times 0.1^\circ$	1 h	<i>DSWR</i> , Albedo, <i>DLWR</i> , <i>ULWR</i>	1981-present
GLDAS	NASA	$0.25^\circ \times 0.25^\circ$	3 h	<i>DSWR</i> , Albedo, <i>DLWR</i> , <i>ULWR</i>	2000-present
<i>Satellite</i>					
GLASS products	University of Maryland	$0.05^\circ \times 0.05^\circ$	1 day 8 days	<i>DSWR</i> Albedo	2000-2017
CERES-SYN	NASA	$1^\circ \times 1^\circ$	1 day	<i>Ro</i>	2000-present
<i>Observation</i>					
OBS-Brazil	University of Texas/Universidade Federal de Espirito Santo	$0.25^\circ \times 0.25^\circ$	1 day	<i>DSWR</i>	1980-2017
		$0.1^\circ \times 0.1^\circ$		<i>Ta</i>	

contains daily records of T_a and $DSWR$ from 735 weather stations across Brazil. These were interpolated in a grid of $0.25^\circ \times 0.25^\circ$ for $DSWR$ and $0.1^\circ \times 0.1^\circ$ for T_a , in the 1980-2017 period (Xavier *et al.*, 2016). For conventional stations, $DSWR$ was estimated using the Ångström-Prescott equation, while at automatic stations, $DSWR$ was directly measured using Eppley thermopile pyranometers.

2.4. Radiation Balance (RB)

The RB can be defined, by its four components, as the difference between incoming and outgoing energies at the Earth surface, expressed as:

$$RB = DSWR(1 - \alpha) + (DLWR - ULWR) \quad (1)$$

With the exception of albedo (dimensionless), all components were calculated in W/m^2 . The $DSWR$ is the radiation received directly or indirectly from the sun by a horizontal plane on the Earth's surface, and was extracted from the ERA5-Land, GLDAS and GLASS datasets. Albedo is the fraction of $DSWR$ reflected by the Earth's surface, supplied by the ERA5-Land, GLDAS and GLASS datasets. The $ULWR$ refers to longwave radiation emitted by the Earth's surface towards the atmosphere, extracted from the ERA5-Land and GLDAS datasets. The $DLWR$ is the longwave radiation emitted by the atmosphere towards the Earth's surface, calculated by the ERA5-Land and GLDAS datasets, and through an adaptation of the SEBAL algorithm. This methodology was proposed by Bastiaanssen *et al.* (1998) to calculate the energy balance on surface, and the $DLWR$ is obtained by:

$$DLWR = \sigma \varepsilon_a T_a \quad (2)$$

$$\varepsilon_a = 0.85(-\ln \tau)^{0.09} \quad (3)$$

where σ is Stephen-Boltzmann constant ($5.6697 \times 10^{-8} W/m^2.K^4$), ε_a represents the atmospheric emissivity, T_a (K) was taken from Xavier dataset, and τ is the one way atmospheric transmissivity, which is calculated in this study as the relationship between solar radiation incident on the surface and at the top of the atmosphere, using the following equation:

$$\tau = \frac{DSWR}{R_o} \quad (4)$$

where $DSWR$ and R_o were extracted from Xavier dataset and CERES-SYN, respectively.

2.5. Statistic validation

The performance of the datasets in the calculation of the RB components was determined by comparison reanalyses, satellite-based and blended data with USR, PDG and Marambaia observations. Four statistical indices were

used: correlation coefficient (r), bias, root-mean-square error (RMSE) and mean relative error (MRE). The linear relationship between estimates and observations is explain by r . The bias is the tendency to overestimate or underestimate the error. The RMSE is the general error in the predictions in relation to the actual observed value. The MRE is a measure of forecast accuracy, expressed as a percentage. These statistical indices are widely used in validation studies of the RB components (Ferreira *et al.*, 2020; Oliveira *et al.*, 2016; Silva *et al.*, 2015; Verma *et al.*, 2016; Zeng *et al.*, 2020). It is noteworthy that, although there are few stations in relation to the size of the territory, they represent different soil cover conditions, environmental and, in particular, distinct weather and cloud conditions in the study area.

To understand the variations of each evaluated products, the main variables that influence the RB components are analyzed. Previous studies show that $DSWR$, Albedo, $DLWR$ and $ULWR$ are strongly determined by cloud cover fraction (CF), enhanced vegetation index (EVI), T_a and land surface temperature (LST), respectively (Jiao *et al.*, 2015; Oliveira *et al.*, 2018; Wang *et al.*, 2018; Wild, 2016; Zuluaga *et al.*, 2021). Except for T_a (directly measured at all stations) the other variables were obtained from MODIS sensor products.

3. Results and discussion

3.1. $DSWR$

The $DSWR$ is the basic energy for biological, physical and chemical processes (Zhang *et al.*, 2020), as well as being an increasingly attractive resource to meet growing energy demands through photovoltaic energy conversion (Wild *et al.*, 2015). For validation of the $DSWR$, Table 2 shows the performance results of ERA5-Land, GLDAS and GLASS to estimate $DSWR$ with respect to stations. Figure 2 shows the comparison between observations and the datasets based on scatterplots analyses.

The standard deviation (SD) indicates that the monthly variability of datasets ranges from 30% to 40%, compared to their annual mean values (Table 2). ERA5-Land shows a statistically significant underestimation of $DSWR$ for all stations (Fig. 2a-c, Table 2). GLDAS and GLASS do not present statistically significant bias, except for GLDAS at the PDG station (bias = $10 W/m^2$, Table 2). Differences between GLASS and GLDAS are evident when analyzing the error values, which is smaller in GLASS (Table 2). The latter displays values of $RMSE < 40 W/m^2$ and $MRE < 18\%$ for all stations, while the lowest GLDAS values are $RMSE = 43 W/m^2$ at PDG and $MRE = 21\%$ at USR. ERA5-Land presents the largest errors at the Marambaia station ($RMSE = 93 W/m^2$ and $MRE = 49\%$) and the smallest at the PDG station ($RMSE = 55 W/m^2$ and $MRE = 25\%$), still much larger

Table 2 - Statistic performance of datasets to estimate *DSWR* compared to the observations (Obs) from stations. Values in bold indicate significant values at 95% level (p-value ≤ 0.05).

Station	Obs	ERA5-Land	GLDAS	GLASS
<i>USR</i>				
Mean (W/m ²)	222	170	222	214
SD (W/m ²)	71	50	66	64
r		0.7	0.8	0.9
Bias (W/m ²)		-52	0	-8
RMSE (W/m ²)		71	44	32
MRE (%)		29	20	12
<i>PDG</i>				
Mean (W/m ²)	213	172	223	216
SD (W/m ²)	63	50	64	66
r		0.8	0.8	0.9
Bias (W/m ²)		-42	10	3
RMSE (W/m ²)		55	43	32
MRE (%)		25	21	13
<i>Marambaia</i>				
Mean (W/m ²)	191	160	190	194
SD (W/m ²)	76	61	61	79
r		0.2	0.8	0.9
Bias (W/m ²)		-31	-1	2
RMSE (W/m ²)		93	45	38
MRE (%)		49	28	17

than those presented by GLASS. Verifying the ERA5-Land at the USR station, the r values (0.7-0.9) suggests a moderate-strong relationship between the datasets and observations (Table 2). Among all datasets, GLASS displays the highest concentration of scatter points on the 1:1 line in the three stations (Fig. 2).

The comparison between gridded products and local station measurements can induce errors, because the pixel assumes unique values for spatially heterogeneous surface, which may not correspond to the observations surface type (Huang *et al.*, 2016). Thus, spatial resolution plays an important role, as in the case of GLDAS, where the proper scatter (Fig. 2d-f), may be related to its grid (0.25° lat/lon), as argued by Oliveira *et al.* (2016) in the Amazon. However, ERA5-Land, despite having a more refined spatial resolution (0.1° lat/lon), presents larger scattering (Fig. 2a-c) and higher errors (Table 2) in comparison to other datasets.

Figure 3 presents the daily *DSWR* variability by month in the three stations. As expected, the maximum values of observed *DSWR* (362 W/m² at USR, 340 W/m² at PDG, and 371 W/m² at Marambaia), is observed for the austral summer. This season takes place between December and February, when the solar zenith angle over the Southern Hemisphere is the lowest and, therefore, more radiation is received at the top of the atmosphere. The

minimum values of observed *DSWR* appear in September, in the beginning of spring (26 W/m² at USR and 25 W/m² at PDG), and in July, during winter (34 W/m² at Marambaia). All datasets are able to reproduce the *DSWR* seasonal variability. During summer, the highest *DSWR* values are displayed, as well as greater variability (longer box plots), associated with changes in rainfall and cloudiness, caused by South American Monsoon (SAM). This, begins at Equatorial Amazon in the spring, and spreads rapidly to the east and southeast of the country during summer, boosting the SACZ (Garcia and Kayano, 2015). In contrast, in winter, the lowest *DSWR* values and the least variability (shorter box plots) are shown, related to the dry season and the cloudless sky that mark the end of SAM (Garcia and Kayano, 2015). In this period the cloudiness of the southeastern region results from the presence of substantially cold frontal systems (Zandonadi *et al.*, 2015).

Considering that Zuluaga *et al.* (2021) found that cloud cover is the main factor that contributes to the *DSWR* variations in southeastern Brazil, Fig. 4 shows the correlation between cloud fraction (CF), and the observed and estimated *DSWR* standard deviation. At the USR (Fig. 4a) and PDG (Fig. 4b) stations, values of r (> 0.8) indicate that, in general, datasets are able to simulate the strong influence that CF has on *DSWR* variations. In these two seasons, ERA5-Land presents the main lags in the spring-summer transition (October-December), when SACZ starts to act on the region. The Marambaia station (Fig. 4c) exhibits greater CF variability, probably related to constant advection from the ocean, making it more difficult for datasets simulations. Here, ERA5-Land and GLDAS show difficulty in simulating *DSWR* variability during spring and much of summer (December and January). GLASS displays correlation values closer to the observations, with some differences during autumn and winter, when CF is mainly related to frontal systems.

In short, the combination of geostationary and polar orbit satellites, high spatial resolution, and algorithms for different cloud conditions, makes GLASS the best option for *DSWR* studies in southeastern Brazil. In addition to the previous one, all datasets are restricted to continental areas, which should influence the large errors presented in pixels near the coast (Kara *et al.*, 2007; Pelosi *et al.*, 2020), as in the case of the Marambaia station.

3.2. Albedo

Albedo is a fundamental parameter of the RB; since it controls the energy budget through the regulation of the *DSWR* quantity reflected by the surface (He *et al.*, 2018). Table 3 contains the statistical analyses of the datasets in estimating the surface albedo. Figure 5 shows the scatter-plots between observed and estimated albedo from the datasets.

Estimates of albedo at the USR station deliver the largest errors among the 3 stations (Table 3) with the worst

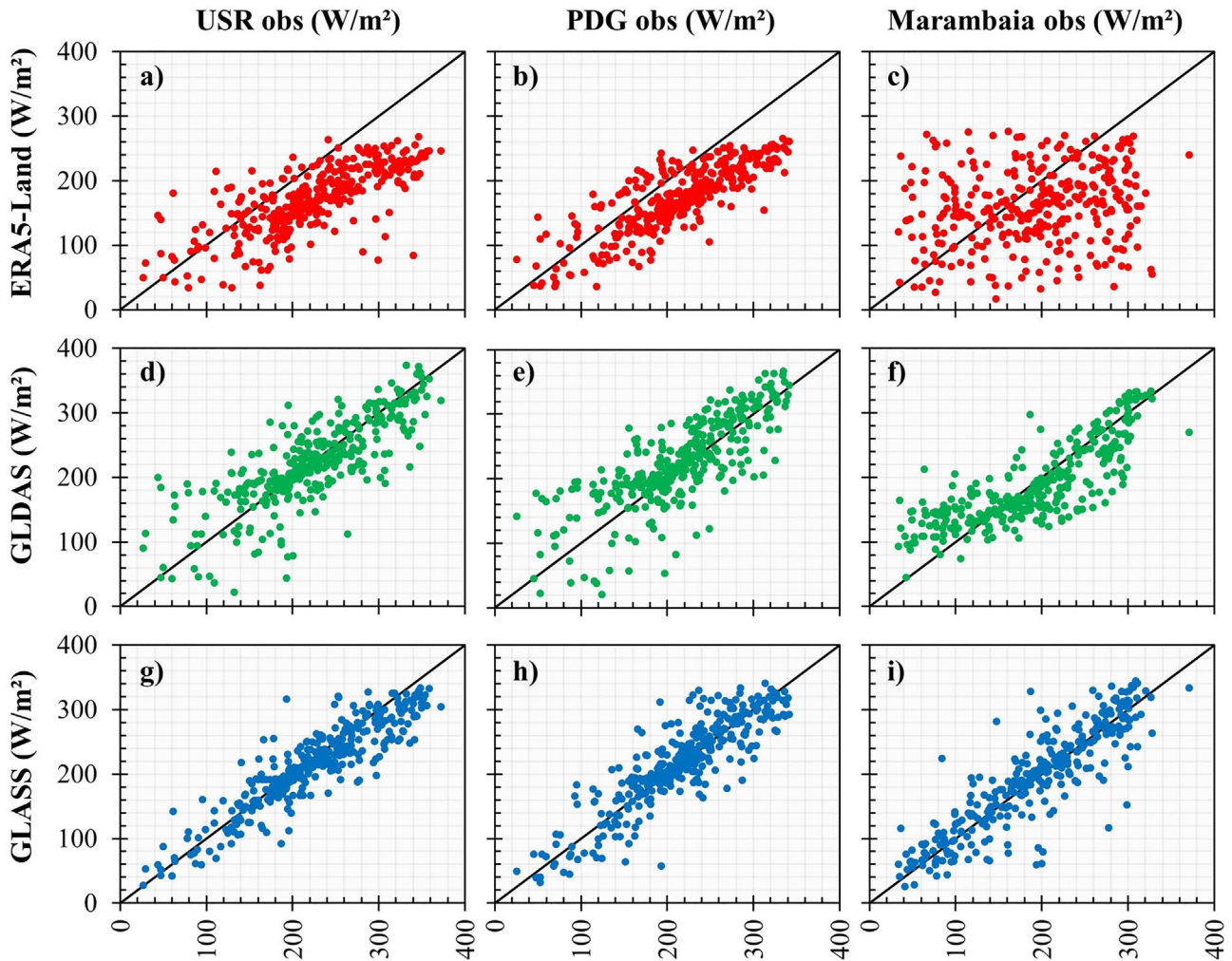


Figure 2 - Comparison between *DSWR* estimations from datasets and observed in USR (a, d, g), PDG (b, e, h) and Marambaia (c, f, i) stations. ERA5-Land is red, GLDAS is green and GLASS is blue.

results for GLDAS (RMSE = 0.067, MRE = 34.059%), followed by GLASS (RMSE = 0.064, MRE = 32.615%) and ERA5 -Land (RMSE = 0.039, MRE = 18.739%). Observed data show a mean albedo of 0.189 but varying substantially during the studied period (SD = 0.016). These values are underestimated by the datasets with a mean bias of -0.054 (Table 3), and a concentration of scatter points below the 1: 1 line (Fig. 5a). Despite these results, GLDAS and ERA5-Land show positive statistically significant correlations.

At the PDG station, biases (Table 3) show a reasonable performance for ERA5-Land (0.003) but statistically significant underestimation of albedo for GLDAS (-0.0048) and GLASS (-0.022). Moreover, these datasets do not follow the high variability of the observations as demonstrated by reduced standard deviation (SD = 0.018). ERA5-Land and GLDAS show negative correlations, but not statistically significant. The RMSE range from 0.020 to 0.051, and the MRE from 10.351% to 29.152%

(Table 3). The low variability of the datasets is reflected in the line-shaped scatterplot in Fig. 5b.

In opposite to that has been found for the *DSWR* (Section 3.1), at the Marambaia station the best agreement is found for albedo estimates among the datasets (Table 3). These results are explained, in part, by the low variability of observations (SD = 0.009), which perhaps can be better treated by the reanalysis and satellite data. GLASS has the highest correlation ($r = 0.695$), while ERA5-Land exhibits a negative and statistically significant correlation ($r = -0.407$). The scatters in Fig. 4c show the reasonable fit between GLASS and observations, as shown by a bias close to 0 (Table 3). The GLASS delivers the smallest errors (RMSE = 0.006, MRE = 3.592%) and GLDAS and ERA5-Land outperformed GLASS errors by almost 5 times (Table 3).

Considering that the albedo depends on the characteristics of the surface (vegetation in this case), each station is discussed separately. For this, Fig. 6 shows the

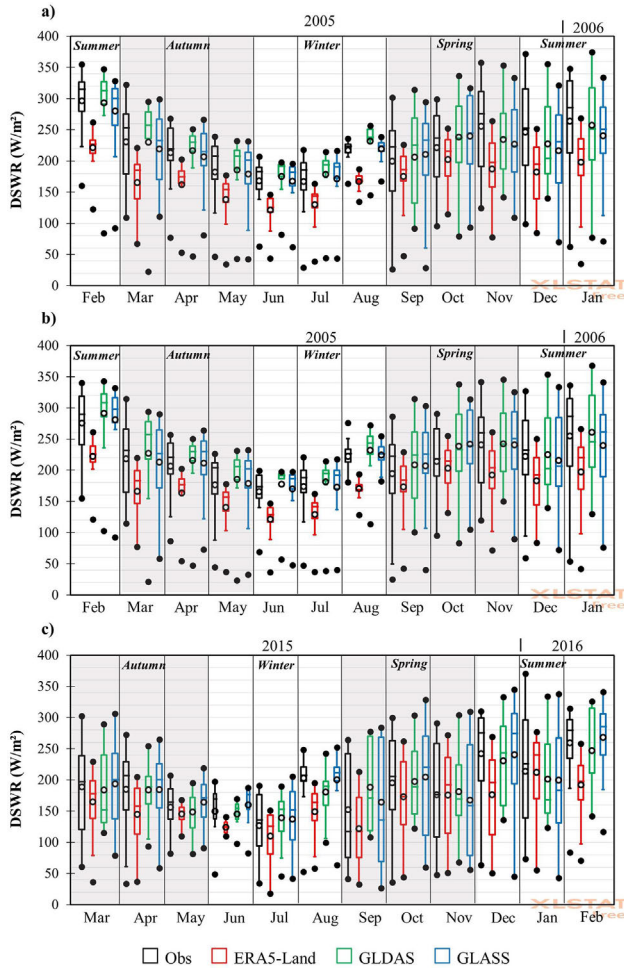


Figure 3 - Variability of daily $DSWR$ by month in the a) USR, b) PDG and c) Marambaia stations from observations and datasets. Box plot include the interquartile range (25th-75th percentiles), median (horizontal line), mean (black circles), maximum and minimum values (black dots).

variability of albedo and the enhanced vegetation index (EVI) by month in the three stations. EVI is a frequently used remote-sensing vegetation phenological metric, which is optimized to resist atmospheric and soil background effects (Wang *et al.*, 2017).

In February (regrowth phase), due to the absence of leaves, the higher reflectance of the soil determines and contributes to the highest (lower) albedo (EVI) value of the period ($\alpha = 0.22$, $EVI = 0.26$) (Oliveira *et al.*, 2018; Williamson *et al.*, 2016). Between March and July, during the tillering phase, albedo decreases to approximately 0.19 related to the appearance and development of sprouts, leading to larger EVI up to 0.42. Between August and September, the albedo continues to decrease until 0.17 due to the total coverage of the soil by the foliage of the plants ($EVI = 0.46$) favoring absorption of solar radiation. Finally, between December and January, the maturation and senescence of the leaves appear ($EVI = 0.41$), and the

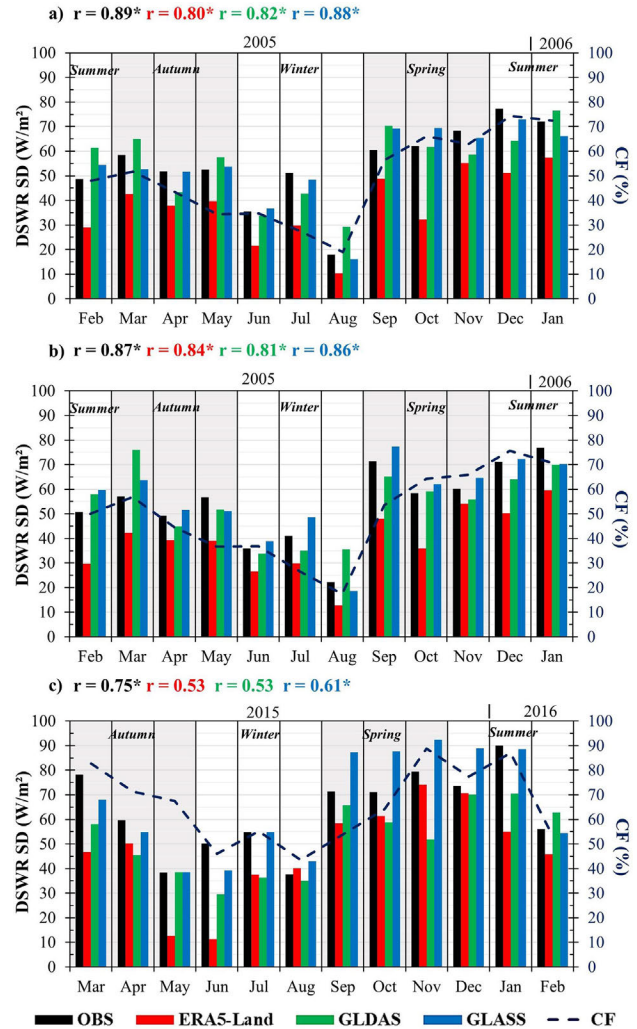


Figure 4 - Correlation (r) between monthly cloud fraction (CF) from MOD08_M3 and standard deviation (SD) of $DSWR$, in the a) USR, b) PDG and c) Marambaia stations. Significant r values at 95% level (p -value ≤ 0.05) are accompanied by *.

albedo value returns to values close to 0.20 (Fig. 6a). These results are in line with those found by Oliveira *et al.* (2018) and Scarpate *et al.* (2016).

The PDG station presents the highest albedo values ($\alpha \approx 0.17$) during the spring when the renewal of the foliage generates greater vegetative vigor ($EVI = 0.42$). The lowest albedo values ($\alpha \approx 0.15$) correspond to autumn/winter (Fig. 5b). According to Oliveira *et al.* (2018), the reduction in albedo is due to the fact that during the dry season (winter) $DSWR$ penetrates the canopy more easily due to less foliage ($EVI = 0.35$), and the soil covered by dark plant litter absorbs more radiation.

According to Carvalho *et al.* (2015), the characteristic vegetation that surrounds the Marambaia station, presents its peak of leaf fall during the dry season (July-September) and beginning of the rainy season (October-November) with mean EVI value of 0.45. This, together

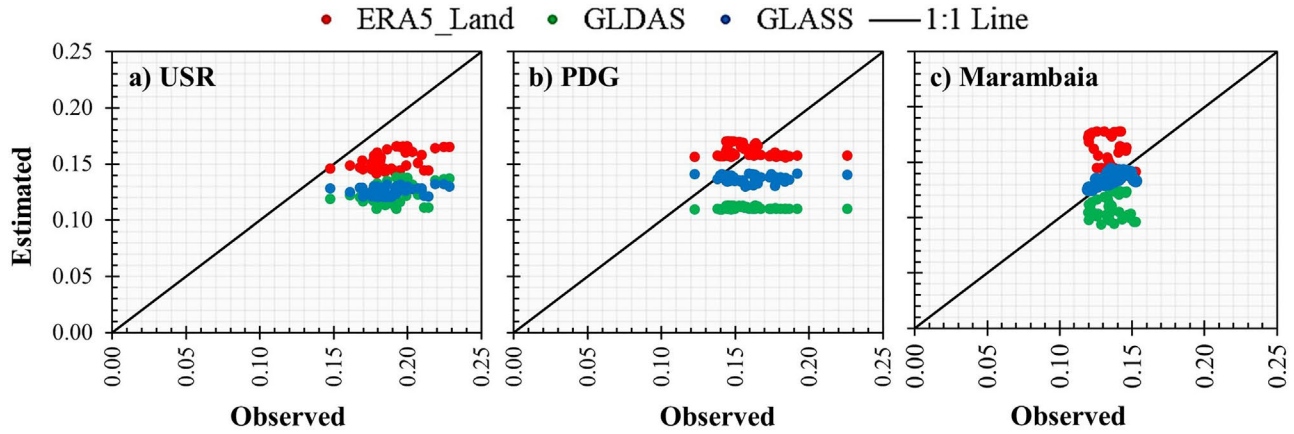


Figure 5 - Comparison between albedo estimations from datasets and observed in a) USR, b) PDG and c) Marambaia stations.

Table 3 - Statistic performance of datasets to estimate albedo (α) compared to observations (Obs) from stations. Values in bold indicate significant values at 95% level (p -value ≤ 0.05).

Station	Obs	ERA5-Land	GLDAS	GLASS
<i>USR</i>				
Mean	0.189	0.153	0.124	0.126
SD	0.016	0.009	0.009	0.004
r		0.445	0.352	0.275
Bias		-0.036	-0.065	-0.062
RMSE		0.039	0.067	0.064
MRE (%)		18.739	34.059	32.615
<i>PDG</i>				
Mean	0.159	0.162	0.111	0.137
SD	0.018	0.005	0.001	0.003
r		-0.275	-0.225	0.012
Bias		0.003	-0.048	-0.022
RMSE		0.020	0.051	0.028
MRE (%)		10.351	29.152	13.397
<i>Marambaia</i>				
Mean	0.135	0.156	0.109	0.135
SD	0.009	0.014	0.010	0.006
r		-0.407	0.073	0.695
Bias		0.020	-0.026	0.000
RMSE		0.028	0.029	0.006
MRE (%)		17.154	18.932	3.592

with the high content of organic matter in the soil, contributes to the reduction of albedo to 0.12 (Fig. 5c). However, between December and June, the vegetation has its greatest vegetative vigor ($EVI \approx 0.56$) reaching an albedo of up to 0.15.

Turning to the GLDAS product is noticed that it is able to reproduced the albedo seasonality pace at USR and Marambaia stations, but with a clear underestimation (Fig. 6a, c). At the PDG station, albedo is also underestimated and remains practically constant throughout the

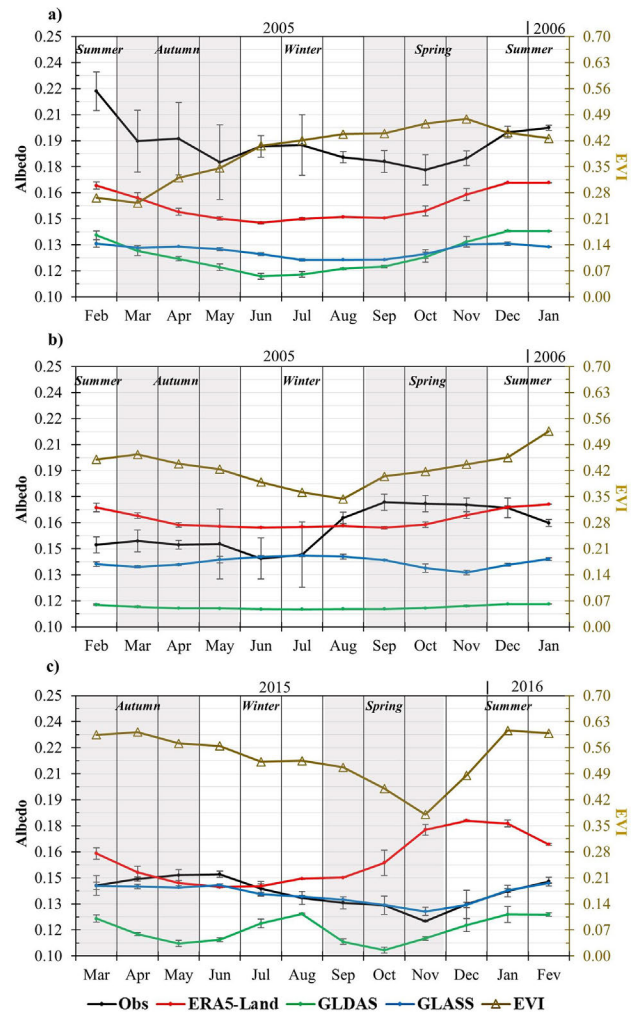


Figure 6 - Variability of monthly EVI from MOD13Q1 and weekly albedo by month in the a) USR, b) PDG and c) Marambaia stations from observations and datasets. Error lines correspond to standard deviation.

year (Fig. 6b). These values may be associated with the fact that the GLDAS uses a global static land cover dataset, based on observations from the AVHRR in 2000 (Ro-

dell *et al.*, 2004). ERA5-Land presents practically the same albedo cycle (with the similar values) at USR and PDG stations (Fig. 6a-b), which leads to the conclusion that despite its high resolution there is no differentiation between USR and PDG land cover. At Marambaia station an out-of-phase pattern of the albedo is shown with respect to observations (Fig. 6c). This is very likely related to caveats in ERA5-Land along coastline regions primarily reproducing sea-land mean albedo (Pelosi *et al.*, 2020). GLASS matches the seasonal variations of observed albedo in the 3 stations (Fig. 6), but values are underestimated in USR and PDG (Fig. 6a-b). According to Liu *et al.* (2013), GLASS presents deficiencies related to the quantity (and quality) of data that is applied to training the regression algorithms used to calculate the albedo, mainly in tropical areas.

Additionally, two factors must be considered: 1) albedo observations are local, while GLDAS and GLASS use satellites, whose nominal resolution may be 1 km, but generally perform spatial averages to remove the effects of cloudiness. 2) Satellite detection leads to a sensitivity limit in the decimals of the albedo values and even to systematic errors. These two facts help to understand that the albedos observed by GLDAS and GLASS are practically constant throughout the year.

3.3. DLWR

The *DLWR*, also known as thermal infrared energy, is considered a fundamental indicator of the effect of atmospheric greenhouse gases (water vapor, CO₂, etc.) on the climate (Tang *et al.*, 2021). However, *DLWR* observations are rarely available due to the cost of the instruments for their measurement (Kruk *et al.*, 2010). Figure 7 shows the comparison of daily *DLWR* estimates and observed values. The statistical results of the comparisons are summarized in Table 4.

The observed values show that the *DLWR* variability (SD) at the Marambaia station is twice as high as at the USR station (Table 4). The *r* values of all datasets are statistically significant, however, at USR, the correlations are strong ($r \geq 0.7$), while at Marambaia this is moderate-weak ($0.4 \leq r \leq 0.5$). The complexity of estimating *DLWR* leads to different biases among datasets. ERA5-Land presents statistically significant bias, with overestimation at USR (bias = 14 W/m²) and underestimation at Marambaia (bias = -4 W/m²). GLDAS and SEBAL show completely different biases with values between -4 and 2 W/m² (without statistical significance) at USR, and underestimations between -45 and -26 W/m² (with statistical significance) at Marambaia (Table 4). The GLDAS, however shows the best fit with the observed *DLWR* at USR (Fig. 7b). It should be noted that at both stations (Table 4).

Figure 8 shows observed and estimated temporal variability of *DLWR*. Largest *DLWR* are noted in the USR (≈ 375 W/m²) and Marambaia (≈ 420 W/m²) stations du-

Table 4 - Statistic performance of datasets to estimate *DLWR* compared to station observations (Obs). Values in bold indicate significant values at 95% level (p-value ≤ 0.05).

Station	Obs	ERA5-Land	GLDAS	SEBAL
<i>USR</i>				
Mean (W/m ²)	356	370	358	352
SD (W/m ²)	33	29	32	18
<i>r</i>		0.9	0.9	0.7
Bias (W/m ²)		14	2	-4
RMSE (W/m ²)		18	14	17
MRE (%)		4	3	4
<i>Marambaia</i>				
Mean (W/m ²)	413	410	387	369
SD (W/m ²)	17	25	26	17
<i>r</i>		0.4	0.4	0.5
Bias (W/m ²)		-4	-26	-45
RMSE (W/m ²)		24	36	48
MRE (%)		5	7	11

ring spring/summer, in agreement to maximum cloudiness and precipitation across the Southeast region (Coelho *et al.*, 2016). In opposite, the lowest *DLWR* values appear during the dry period (autumn/winter), with ≈ 320 W/m² at USR, and ≈ 398 W/m² at Marambaia (Fig. 8). This pattern is associated with the fact that the emissivity and atmospheric temperature (see Eq. (2)) present their maximum values during summer, and minimum values in winter (Ferreira *et al.*, 2012). The influence of water vapor should not be disregarded. For instance, higher *DLWR* values at Marambaia station is associated with maritime advection of water vapor onto the continent in line with the sea breeze effect. This might increase the atmospheric humidity inducing higher *DLWR* (Brito and Oyama, 2014; Marques *et al.*, 2010).

According to Wang *et al.* (2018), even on cloudy-sky days, *Ta* is a main controlling factor that influences the surface *DLWR*. Figure 9 shows the correlation between *Ta* and *DLWR*, measured at each station. Both places show high and statistically significant correlations ($r > 0.8$). At the USR station (Fig. 9a), observed and estimated *DLWR* fit nicely the pace of the *Ta* seasonal cycle. In Marambaia (Fig. 9b) disagreements between observation and estimation are exhibited during autumn and winter, probably due to limitation of ERA5-Land and blended data to reproduce the *Ta* daily variability. In this period, air temperatures may be affected by periodic stratocumulus clouds. During the spring/summer, *DLWR* from ERA5-Land matches the observations. The weak seasonal march of *Ta* in Marambaia is also reflected in the low variability of *DLWR*. In general, with all limitation, the datasets are able to capture the *DLWR* seasonality in both stations. However, caution should be taken if these data have to be used on high frequency, such as daily values.

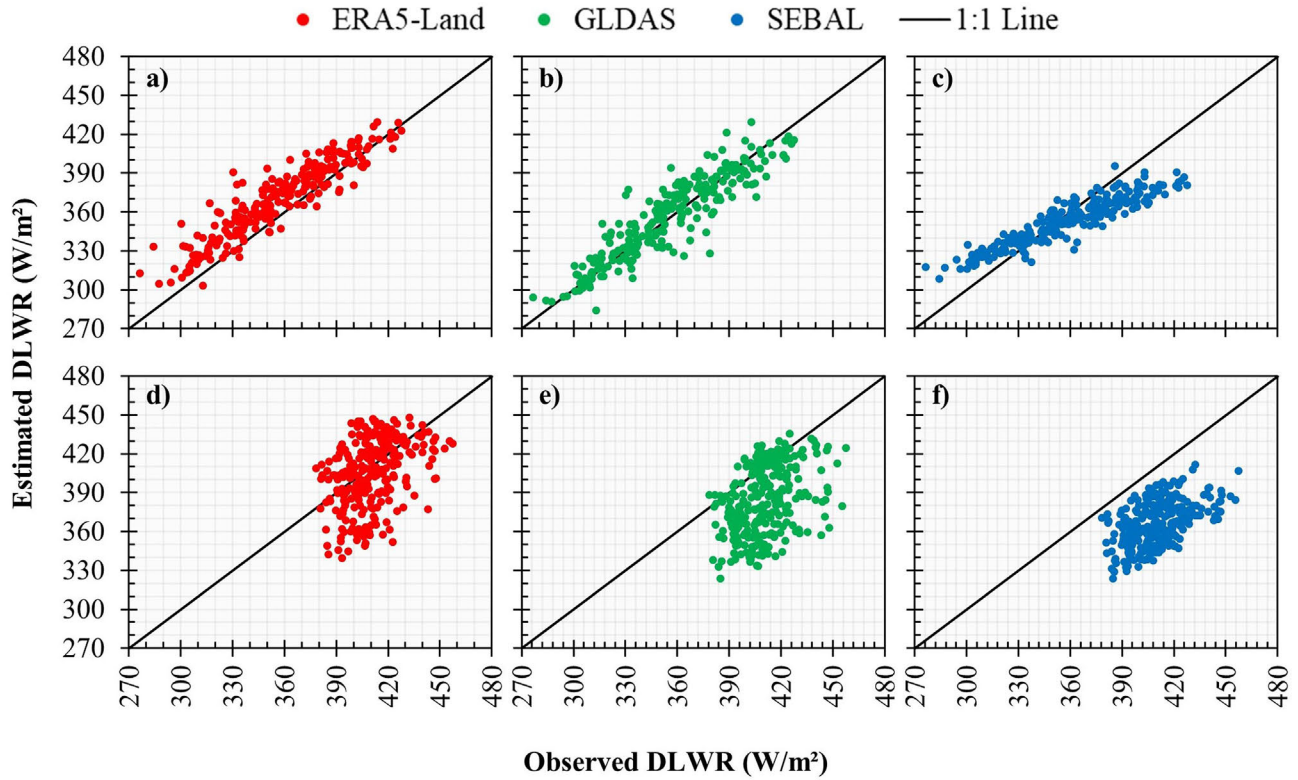


Figure 7 - Comparison between *DLWR* estimations from datasets and observed in USR (a-c) and Marambaia (d-f) stations.

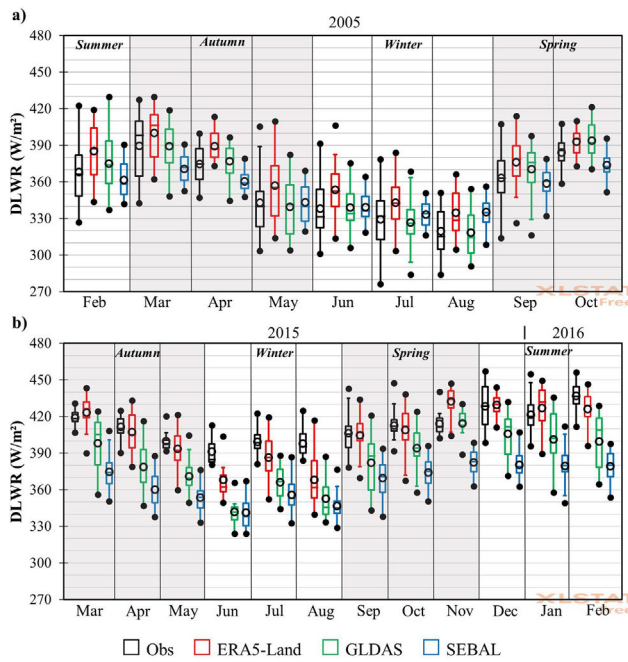


Figure 8 - Variability of daily *DLWR* by month in the a) USR and b) Marambaia stations from observations and datasets. Box plot include the interquartile range (25th-75th percentiles), median (horizontal line), mean (black circles), maximum and minimum values (black dots).

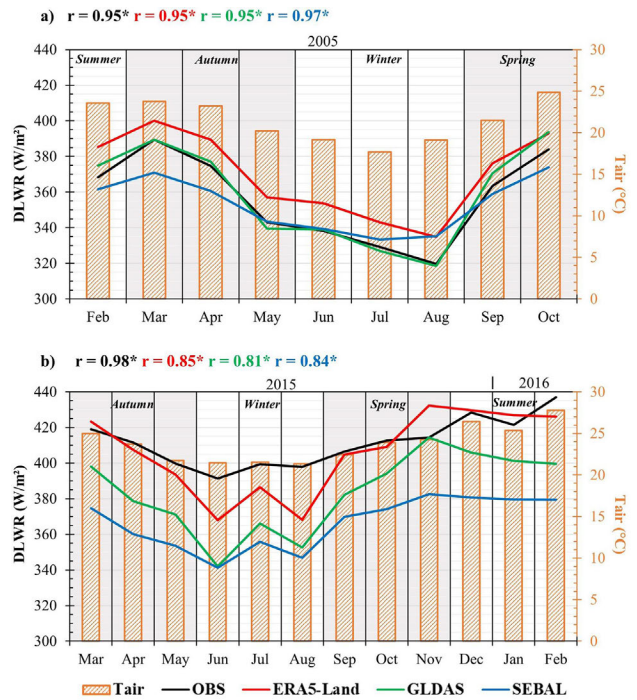


Figure 9 - Correlation (r) between observed monthly air temperature (T_{air}) from a) USR and b) Marambaia stations, and monthly *DLWR*. Significant r values at 95% level (p -value ≤ 0.05) are accompanied by *.

3.4. ULWR

The *ULWR* is the component of the RB that mainly represents the thermal radiation capacity of the Earth's surface, dominating at night, in high latitudes and during most of the year in the Polar Regions (Jiao *et al.*, 2015; Qin *et al.*, 2020). Table 5 and Fig. 10 show the comparison between observed *ULWR* and estimates from two datasets.

Table 5 - Statistic performance of datasets to estimate *ULWR* compared to station observations (Obs). Values in bold indicate significant values at 95% level (p-value ≤ 0.05).

Station	Obs	ERA5-Land	GLDAS
<i>USR</i>			
Mean (W/m ²)	433	436	421
SD (W/m ²)	16	19	19
r		0.8	0.8
Bias (W/m ²)		3	-12
RMSE (W/m ²)		10	16
MRE (%)		2	3
<i>Marambaia</i>			
Mean (W/m ²)	443	449	432
SD (W/m ²)	26	17	16
r		0.2	0.2
Bias (W/m ²)		6	-12
RMSE (W/m ²)		28	30
MRE (%)		5	5

Observations and reanalyses show variability (SD) between 3% and 5% in relation to the mean *ULWR* values in the two stations (Table 5). The correlations in USR (0.8) are higher than in Marambaia (0.2), statistically significance in both stations. Biases values show that ERA5-Land slightly overestimates *ULWR* in both stations

(3 W/m² at USR, 6 W/m² at Marambaia). However, the high scatter of *ULWR* estimated at Marambaia station (Fig. 10b) is reflected in larger errors (RMSE = 28 W/m², MRE = 5%) than those presented at USR station (RMSE = 10 W/m², MRE = 2%). GLDAS has a similar behavior to ERA5-Land, with greater scattering of *ULWR* estimated at Marambaia with respect to that delivered by the USR (Fig. 10c-d); but with a tendency of underestimation in both stations (mean bias = -12 W/m², Table 5). The errors shown by GLDAS, both at USR (RMSE = 16 W/m², MRE = 3%) and at Marambaia (RMSE = 30 W/m², MRE = 5%), slightly exceed those of ERA5-Land.

The variability of *ULWR* over the measurement period at the two stations is shown in Fig. 11. Similar to *DLWR* (Section 3.3), the highest observed *ULWR* values correspond to spring/summer (≈ 440 W/m² at USR, ≈ 455 W/m² at Marambaia). The smallest amount of observed *ULWR* is noticed during autumn/winter (≈ 420 W/m² at USR, ≈ 435 W/m² at Marambaia). According to Teixeira *et al.* (2015), *ULWR* is mainly determined by the land surface temperature (*LST*) - which

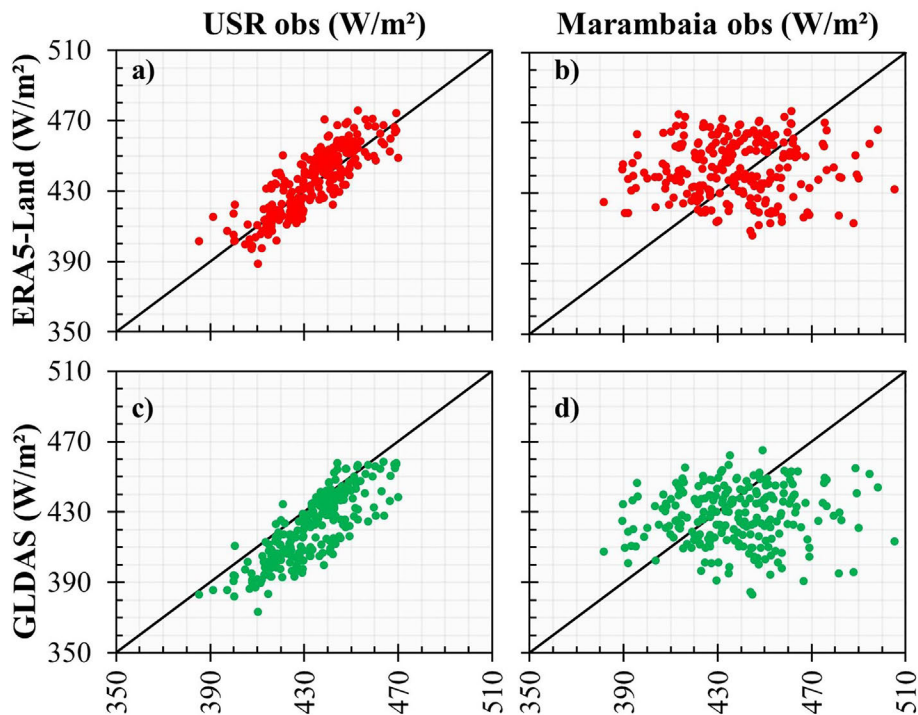


Figure 10 - Comparison between *ULWR* estimations from datasets and observed in USR (a,c) and Marambaia (b,e) stations. ERA5-Land is red and GLDAS is green.

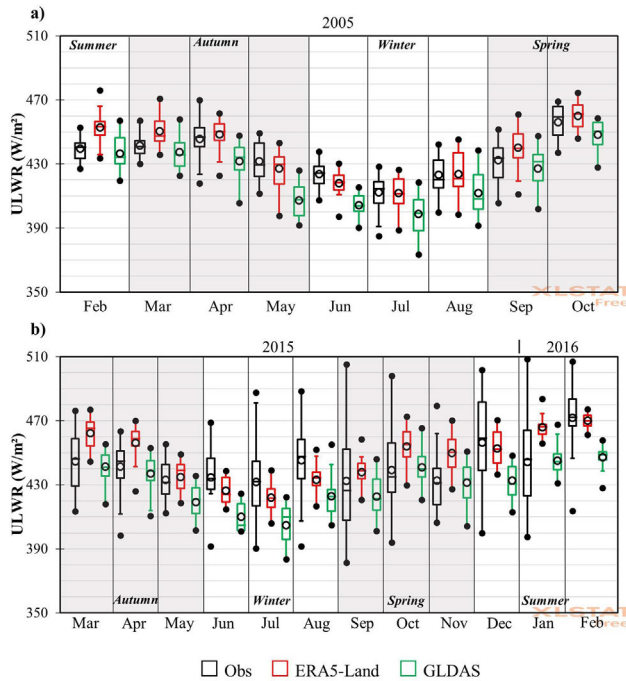


Figure 11 - Variability of daily *ULWR* by month in the a) USR and b) Marambaia stations from observations and datasets. Box plot include the interquartile range (25th-75th percentiles), median (horizontal line), mean (black circles), maximum and minimum values (black dots).

depends on the *DSWR* amount - unlike the albedo which essentially depends on the type of ecosystem and the surface humidity conditions.

In this sense, Fig. 12 shows the correlation between *LST* and *ULWR*. At the USR station (Fig. 12a); it is clear that the good performance of the datasets is related to the strong correlation ($r > 0.94$) that exists between the *ULWR* and *LST* cycles. In Marambaia (Fig. 12b), although the correlations are moderate ($0.59 \leq r \leq 0.72$), they are statistically significant. The main differences shown by the datasets are related to the underestimation of the effect of *LST* on *ULWR*, mainly in the case of GLDAS, and with some disagreements in the direction of the variations during the spring/summer especially. The optimal performance of datasets in the *ULWR* estimate, can be related to the fact that *LST*, in ERA5-Land and GLDAS, is one of the most accurate variables in relation to reality, due to the correction of bias in the data assimilation processes (Hersbach et al., 2020; Rodell et al., 2004). The slight advantage of ERA5-Land may be related to its high resolution (0.1°) compared to GLDAS (0.25°).

4. Conclusions

In this study, several datasets were evaluated on the southeast region of Brazil, which is a region with abrupt environmental changes caused by its economic growth and high population density. The components of the radia-

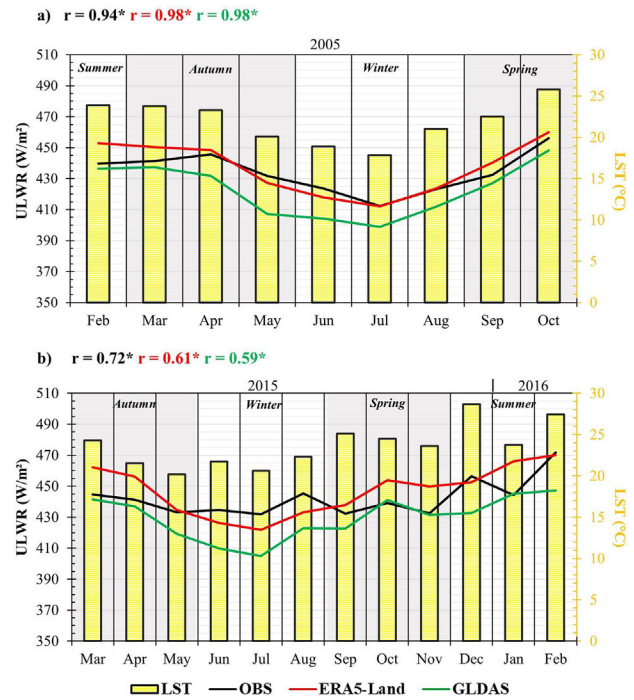


Figure 12 - Correlation (r) between Land Surface Temperature (*LST*) from MOD11C3 and monthly mean *ULWR* in the a) USR and b) Marambaia stations. Significant r values at 95% level (p -value ≤ 0.05) are accompanied by *.

tion balance from five datasets (obtained directly or indirectly) were compared with observations from three stations, located inside surfaces with different physical characteristics. For this, we use indicators that estimate the accuracy of the datasets (r , bias, RMSE and MRE).

The results showed that ERA5-Land offered the best performance in estimating albedo, *DLWR* and *ULWR*. In the case of *DSWR*, GLASS delivered the most accurate values in relation to the observations. Both datasets proved to be an adequate alternative to estimate the components of the radiation balance in southeastern Brazil.

For the *DSWR*, *DLWR* and *ULWR* components, the datasets presented the biggest errors in the Marambaia station, probably because these are products restricted to the land areas. These products can also be subject to parameterization errors in the radiative transfer models, such as limitations to capture variations generated by dominant meteorological systems (cloud changes) in the spring/summer period. Albedo was the most problematic component due to the low seasonal variability shown by datasets in all stations. The worst albedo results were observed in the USR station, which corresponds to a sugarcane field. The datasets were unable to accompany the high variability of albedo due to the phenological cycles of the crop.

Analyzes conducted in this study highlight uncertainties that still represent posing a challenge for the research community in the development of products that compute the radiation balance components. Future studies

should explore the combination or merging of different datasets aiming at correcting errors in the coastal areas and the albedo estimates. Adequate calculations of the radiation balance components will lead to fundamental advances for the hydrological and ecological communities to improve their estimates of sensitive and latent heat, evapotranspiration, gross primary production, and surface climate projections at large.

Acknowledgments

We acknowledge the Coordination for the Improvement of Higher Education Personnel (CAPES) for supporting this research. We acknowledge all the Institutions that make their datasets available. The author thanks the graduate program in Applied Meteorology at the Universidade Federal de Viçosa.

References

- ALVARENGA, L.A.; DE MELLO, C.R.; COLOMBO, A.; CUARTAS, L.A.; BOWLING, L.C. Assessment of land cover change on the hydrology of a Brazilian headwater watershed using the Distributed Hydrology-Soil-Vegetation Model. **Catena**, v. 143, p. 7-17, 2016. doi
- AMATYA, P.; MA, Y.; HAN, C.; WANG, B.; DEVKOTA, L.P. Estimation of net radiation flux distribution on the southern slopes of the central Himalayas using MODIS data. **Atmospheric Research**, v. 154, p. 146-154, 2015. doi
- BASTIAANSEN, W.G.M.; MENENTI, M.; FEDDES, R.A.; HOLTSLAG, A.A.M. A remote sensing surface energy balance algorithm for land (SEBAL). 1. Formulation. **Journal of Hydrology**, v. 212-213, p. 198-212, 1998. doi
- BENGTTSON, L.; ARKIN, P.; BERRISFORD, P.; BOUGEAULT, P.; FOLLAND, C.; *et al.* The need for a dynamical climate reanalysis. **Bulletin of the American Meteorological Society**, v. 88, n. 4, p. 495-502, 2007. doi
- BERNARDINO, B.; VASCONCELLOS, F.; NUNES, A. Impact of the equatorial Pacific and South Atlantic SST anomalies on extremes in austral summer precipitation over Grande river basin in Southeast Brazil. **International Journal of Climatology**, v. 38, p. e131-e143, 2018. doi
- BISHT, G.; BRAS, R. Estimation of net radiation from the MODIS data under all sky conditions: Southern Great Plains case study. **Remote Sensing of Environment**, v. 114, n. 7, p. 1522-1534, 2010. doi
- BISHT, G.; BRAS, R. Estimation of net radiation from the moderate resolution imaging spectroradiometer over the continental United States. **Remote Sensing of Environment**, v. 49, n. 6, p. 2448-2462, 2011. doi
- BISHT, G.; VENTURINI, V.; ISLAM, S.; JIANG, L. Estimation of the net radiation using MODIS (Moderate Resolution Imaging Spectroradiometer) data for clear sky days. **Remote Sensing of Environment**, v. 97, p. 52-67, 2005. doi
- BRITO, S.; OYAMA, M.D. Daily cycle of precipitation over the northern coast of Brazil. **Journal of Applied Meteorology and Climatology**, v. 53, n. 11, p. 2481-2502, 2014. doi
- CAO, B.; GRUBER, S.; ZHENG, D.; LI, X. The ERA5-Land soil-temperature bias in permafrost regions. **The Cryosphere Discussions**, v. 14, p. 2581-2595, 2020. doi
- CARMONA, F.; RIVAS, R.; CASELLES, V. Development of a general model to estimate the net radiation with satellite data on clear-sky days. **Remote Sensing of Environment**, v. 171, n. 2, p. 1-13, 2015. doi
- CARVALHO, A.; SOMNER, G.V.; ALLEN, J. Is the phenology of all restinga species the same? A taxonomically-focused study of Sapindaceae in a highly threatened coastal environment. **Flora**, v. 215, p. 92-101, 2015. doi
- CAVALCANTI, I.F.; FERREIRA, N.J.; SILVA, M.; DIAS, M. **Tempo e Clima no Brasil**. São Paulo: Oficina de Textos 2009
- COELHO, C.A.S.; OLIVEIRA, C.P.; AMBRIZZI, T.; REBOITA, M.S.; CARPENEDO, C.B.; *et al.* The 2014 southeast Brazil austral summer drought: regional scale mechanisms and teleconnections. **Climate Dynamics**, v. 46, n. 11-12, p. 3737-3752, 2016. doi
- CONTE, L.; RENNER, M.; BRANDO, P.; OLIVEIRA DOS SANTOS, C.; SILVÉRIO, D.; *et al.* Effects of tropical deforestation on surface energy balance partitioning in Southeastern Amazonia estimated from maximum convective power. **Geophysical Research Letters**, v. 46, n. 8, p. 4396-4403, 2019. doi
- DIAS, L.C.P.; PIMENTA, F.M.; SANTOS, A.B.; COSTA, M.H.; LADLE, R.J. Patterns of land use, extensification, and intensification of Brazilian agriculture. **Global Change Biology**, v. 22, n. 8, p. 2887-2903, 2016. doi
- DOELLING, D.R.; SUN, M.; NGUYEN, L.T.; NORDEEN, M.L.; HANEY, C.O.; *et al.* Advances in geostationary-derived longwave fluxes for the CERES synoptic (SYN1deg) product. **Journal of Atmospheric and Oceanic Technology**, v. 33, n. 3, p. 503-521, 2016. doi
- DOLINAR, E.K.; DONG, X.; XI, B. Evaluation and intercomparison of clouds, precipitation, and radiation budgets in recent reanalyses using satellite-surface observations. **Climate Dynamics**, v. 46, n. 7-8, p. 2123-2144, 2016. doi
- DRIEMEL, A.; AUGUSTINE, J.; BEHRENS, K.; COLLE, S.; COX, C.; *et al.* Baseline Surface Radiation Network (BSRN): Structure and data description (1992-2017). **Earth System Science Data**, v. 10, p. 1491-1501, 2018. doi
- FERREIRA, M.J.; OLIVEIRA, A.P.; SOARES, J.; CODATO, G.; BÁRBARO, E.W.; *et al.* Radiation balance at the surface in the city of São Paulo, Brazil: diurnal and seasonal variations. **Theoretical and Applied Climatology**, v. 107, n. 1-2, p. 229-246, 2012. doi
- FERREIRA, T.R.; SILVA, B.B.; DE MOURA, M.S.B.; VE-RHOEF, A.; NÓBREGA, R.L.B. The use of remote sensing for reliable estimation of net radiation and its components: a case study for contrasting land covers in an agricultural hotspot of the Brazilian semiarid region. **Agricultural and Forest Meteorology**, v. 291, 2020. doi
- GARCIA, S.R.; KAYANO, M.T. Multidecadal variability of moisture and heat budgets of the South American monsoon system. **Theoretical and Applied Climatology**, v. 121, n. 3-4, p. 557-570, 2015. doi

- GRECCHI, R.C.; GWYN, Q.H.J.; BÉNIÉ, G.B.; FORMAGGIO, A.R.; FAHL, F.C. Land use and land cover changes in the Brazilian Cerrado: A multidisciplinary approach to assess the impacts of agricultural expansion. **Applied Geography**, v. 55, p. 300-312, 2014. doi
- GREEN, J.K.; KONINGS, A.G.; ALEMOHAMMAD, S.H.; BERRY, J.; ENTEKHABI, D.; *et al.* Regionally strong feedbacks between the atmosphere and terrestrial biosphere. **Nature Geoscience**, v. 10, n. 6, p. 410-414, 2017. doi
- HE, T.; LIANG, S.; WANG, D.; CAO, Y.; GAO, F.; *et al.* Evaluating land surface albedo estimation from Landsat MSS, TM, ETM+, and OLI data based on the unified direct estimation approach. **Remote Sensing of Environment**, v. 204, p. 181-196, 2018. doi
- HERSBACH, H.; BELL, B.; BERRISFORD, P.; HIRAHARA, S.; HORÁNYI, A.; *et al.* The ERA5 global reanalysis. **Quarterly Journal of the Royal Meteorological Society**, v. 146, n. 730, p. 1999-2049, 2020. doi
- HUANG, G.; LI, X.; HUANG, C.; LIU, S.; MA, Y.; *et al.* Representativeness errors of point-scale ground-based solar radiation measurements in the validation of remote sensing products. **Remote Sensing of Environment**, v. 181, p. 198-206, 2016. doi
- IBGE - Instituto Brasileiro de Geografia e Estatística. **Contas Regionais do Brasil 2018**. Available from <https://www.ibge.gov.br/estatisticas/economicas/contas-nacionais/9054-contas-regionais-do-brasil.html?=&t=o-que-e>, accessed 5 March 2021.
- INPE - Instituto Nacional de Pesquisas Espaciais. **Sistema de Organização Nacional de Dados Ambientais**. Available from <http://sonda.ccst.inpe.br/>, accessed 11 March 2021.
- JIA, A.; LIANG, S.; JIANG, B.; ZHANG, X.; WANG, G. Comprehensive assessment of global surface net radiation products and uncertainty analysis. **Journal of Geophysical Research: Atmospheres**, v. 123, n. 4, p. 1970-1989, 2018. doi
- JIAO, Z.; YAN, G.; ZHAO, J.; WANG, T.; CHEN, L. Estimation of surface upward longwave radiation from MODIS and VIIRS clear-sky data in the Tibetan Plateau. **Remote Sensing of Environment**, v. 162, p. 221-237, 2015. doi
- KARA, A.B.; WALLCRAFT, A.J.; HURLBURT, H.E. A correction for land contamination of atmospheric variables near land-sea boundaries. **Journal of Physical Oceanography**, v. 37, n. 4, p. 803-818, 2007. doi
- KRUK, N.S.; VENDRAME, I.F.; ROCHA, H.R.; CHOU, S.C.; CABRAL, O. Downward longwave radiation estimates for clear and all-sky conditions in the Sertãozinho region of São Paulo, Brazil. **Theoretical and Applied Climatology**, v. 99, n. 1-2, p. 115-123, 2010. doi
- LIANG, S.; ZHAO, X.; LIU, S.; YUAN, W.; CHENG, X.; *et al.* A long-term Global Land Surface Satellite (GLASS) dataset for environmental studies. **International Journal of Digital Earth**, v. 6, p. 5-33, 2013. doi
- LIU, Q.; WANG, L.; QU, Y.; LIU, N.; LIU, S.; *et al.* Preliminary evaluation of the long-term GLASS albedo product. **International Journal of Digital Earth**, v. 6, p. 69-95, 2013. doi
- MACDOUGALL, A.H.; BELTRAMI, H. Impact of deforestation on subsurface temperature profiles: Implications for the borehole paleoclimate record. **Environmental Research Letters**, v. 12, n. 7, 2017. doi
- MARQUES, W.C.; FERNANDES, E.H.L.; MOLLER, O.O. Straining and advection contributions to the mixing process of the Patos Lagoon coastal plume, Brazil. **Journal of Geophysical Research: Oceans**, v. 115, n. 6, p. 1-23, 2010. doi
- MERCADO, L.M.; BELLOUIN, N.; SITCH, S.; BOUCHER, O.; HUNTINGFORD, C.; *et al.* Impact of changes in diffuse radiation on the global land carbon sink. **Nature**, v. 458, n. 7241, p. 1014-1017, 2009. doi
- MOUKOMLA, S.; BLANKEN, P.D. Estimating the Great Lakes net radiation using satellite remote sensing and MERRA reanalysis. **International Journal of Digital Earth**, v. 10, n. 8, p. 764-784, 2017. doi
- MUÑOZ-SABATER, J.; DUTRA, E.; AGUSTÍ-PANAREDA, A.; ALBERGEL, C.; ARDUINI, G.; *et al.* ERA5-Land: a state-of-the-art global reanalysis dataset for land applications. **Earth System Science Data Discussions**, v. 13, p. 4349-4383, 2021. doi
- OLIVEIRA, B.S.; MORAES, E.C.; CARRASCO-BENAVIDES, M.; BERTANI, G.; MATAVELI, G.A.V. Improved albedo estimates implemented in the METRIC model for modeling energy balance fluxes and evapotranspiration over agricultural and natural areas in the Brazilian Cerrado. **Remote Sensing**, v. 10, n. 8, p. 1181, 2018. doi
- OLIVEIRA, G.; BRUNSELL, N.A.; MORAES, E.C.; BERTANI, G.; DOS SANTOS, T.V.; *et al.* Use of MODIS sensor images combined with reanalysis products to retrieve net radiation in Amazonia. **Sensors**, v. 16, n. 7, p. 956, 2016. doi
- PELOSI, A.; TERRIBILE, F.; D'URSO, G.; CHIRICO, G.B. Comparison of ERA5-Land and UERRA MESCAN-SURFEX Reanalysis Data with spatially interpolated weather observations for the regional assessment of reference evapotranspiration. **Water**, v. 12, n. 6, p. 1669, 2020. doi
- PEREIRA, M.G.; SILVA, A.N.; PAULA, R.R.; MENEZES, L.F.T. Aporte e decomposição de Serapilheira em floresta periodicamente inundável na Restinga da Marambaia, RJ. **Ciencia Florestal**, v. 22, n. 1, p. 59-67, 2012. doi
- QIN, B.; CAO, B.; LI, H.; BIAN, Z.; HU, T.; *et al.* Evaluation of six high-spatial resolution clear-sky surface upward longwave radiation estimation methods with MODIS. **Remote Sensing**, v. 12, n. 11, p. 1834, 2020. doi
- RAMÍREZ-CUESTA, J.M.; VANELLA, D.; CONSOLI, S.; MOTISI, A.; MINACAPILLI, M. A satellite stand-alone procedure for deriving net radiation by using SEVIRI and MODIS products. **International Journal of Applied Earth Observation and Geoinformation**, v. 73, p. 786-799, 2018. doi
- RODELL, M. HOUSER, P.R.; JAMBOR, U.; GOTTSCHALCK, J.; MITCHELL, K.; *et al.* The global land data assimilation system. **Bulletin of the American Meteorological Society**, v. 85, n. 3, p. 381-394, 2004. doi
- SANO, E.E.; ROSA, R.; BRITO, J.L.S.; FERREIRA, L.G. Land cover mapping of the tropical savanna region in Brazil. **Environmental Monitoring and Assessment**, v. 166, n. 1-4, p. 113-124, 2010. doi
- SCARPARE, F.V.; HERNANDES, T.A.D.; RUIZ-CORRÊA, S.T.; PICOLI, M.C.A.; SCANLON, B.R.; *et al.* Sugarcane

- land use and water resources assessment in the expansion area in Brazil. **Journal of Cleaner Production**, v. 133, p. 1318-1327, 2016. [doi](#)
- SILVA, B.B.; MONTENEGRO, S.M.G.; SILVA, V.P.R.; ROCHA, H.R.; GALVÍNCIO, J.D.; *et al.* Determination of instantaneous and daily net radiation from TM - Landsat 5 data in a subtropical watershed. **Journal of Atmospheric and Solar-Terrestrial Physics**, v. 135, p. 42-49, 2015. [doi](#)
- SLATER, A.G. Surface solar radiation in North America: A comparison of observations, reanalyses, satellite, and derived products. **Journal of Hydrometeorology**, v. 17, n. 1, p. 401-420, 2016. [doi](#)
- TANG, W.; QIN, J.; YANG, K.; ZHU, F.; ZHOU, X. Does ERA5 outperform satellite products in estimating atmospheric downward longwave radiation at the surface? **Atmospheric Research**, v. 252, p. 105453, 2021. [doi](#)
- TEIXEIRA, A.H.C.; PADOVANI, C.R.; ANDRADE, R.G.; LEIVAS, J.F.; VICTORIA, D.C.; *et al.* Use of MODIS images to quantify the radiation and energy balances in the Brazilian Pantanal. **Remote Sensing**, v. 7, n. 11, p. 14597-14619, 2015. [doi](#)
- VERMA, M.; FISHER, J.B.; MALLICK, K.; RYU, Y.; KOBAYASHI, H.; *et al.* Global surface net-radiation at 5 km from MODIS Terra. **Remote Sensing**, v. 8, n. 9, p. 739, 2016. [doi](#)
- WANG, C.; LI, J.; LIU, Q.; ZHONG, B.; WU, S.; *et al.* Analysis of differences in phenology extracted from the enhanced vegetation index and the leaf area index. **Sensors (Switzerland)**, v. 17, n. 9, p. 1982, 2017. [doi](#)
- WANG, T.; SHI, J.; YU, Y.; HUSI, L.; GAO, B.; *et al.* Cloudy-sky land surface longwave downward radiation (LWDR) estimation by integrating MODIS and AIRS/AMSU measurements. **Remote Sensing of Environment**, v. 205, p. 100-111, 2018. [doi](#)
- WILD, M. Decadal changes in radiative fluxes at land and ocean surfaces and their relevance for global warming. **Wiley Interdisciplinary Reviews: Climate Change**, v. 7, n. 1, p. 91-107, 2016. [doi](#)
- WILD, M. The global energy balance as represented in CMIP6 climate models. **Climate Dynamics**, v. 55, n. 3-4, p. 553-577, 2020. [doi](#)
- WILD, M.; FOLINI, D.; HENSCHER, F.; FISCHER, N.; MÜLLER, B. Projections of long-term changes in solar radiation based on CMIP5 climate models and their influence on energy yields of photovoltaic systems. **Solar Energy**, v. 116, p. 12-24, 2015. [doi](#)
- WILD, M.; OHMURA, A.; SCHÄR, C.; MÜLLER, G.; FOLINI, D.; *et al.* The Global Energy Balance Archive (GEBA) version 2017: A database for worldwide measured surface energy fluxes. **Earth System Science Data**, v. 9, n. 2, p. 601-613, 2017. [doi](#)
- WILLIAMSON, S.N.; BARRIO, I.C.; HIK, D.S.; GAMON, J.A. Phenology and species determine growing-season albedo increase at the altitudinal limit of shrub growth in the sub-Arctic. **Global Change Biology**, v. 22, n. 11, p. 3621-3631, 2016. [doi](#)
- WOLFE, R.E.; NISHIHAMA, M.; FLEIG, A.J.; KUYPER, J.A.; ROY, D.P.; *et al.* Achieving sub-pixel geolocation accuracy in support of MODIS land science. **Remote Sensing of Environment**, v. 83, n. 1-2, p. 31-49, 2002. [doi](#)
- XAVIER, A.C.; KING, C.W.; SCANLON, B.R. Daily gridded meteorological variables in Brazil (1980-2013). **International Journal of Climatology**, v. 36, n. 6, p. 2644-2659, 2016. [doi](#)
- YU, L.; LIU, T.; CAI, H.; TANG, J.; BU, K.; *et al.* Estimating land surface radiation balance using MODIS in north-eastern China. **Journal of Applied Remote Sensing**, v. 8, n. 1, p. 083523, 2014. [doi](#)
- ZANDONADI, L.; ACQUAOTTA, F.; FRATIANNI, S.; ZAVATTINI, J.A. Changes in precipitation extremes in Brazil (Paraná River Basin). **Theoretical and Applied Climatology**, v. 123, p. 741-756, 2016. [doi](#)
- ZENG, Q.; CHENG, J.; DONG, L. Assessment of the long-term high-spatial-resolution Global Land Surface Satellite (GLASS) surface longwave radiation product using ground measurements. **IEEE Journal of Selected Topics in Applied Earth Observations and Remote Sensing**, v. 13, p. 2032-2055, 2020. [doi](#)
- ZHANG, X.; LIANG, S.; WANG, G.; YAO, Y.; JIANG, B.; *et al.* Evaluation of the reanalysis surface incident shortwave radiation products from NCEP, ECMWF, GSFC, and JMA using satellite and surface observations. **Remote Sensing**, v. 8, n. 3, 2016. [doi](#)
- ZHANG, X.; LIANG, S.; ZHOU, G.; WU, H.; ZHAO, X. Generating Global Land Surface Satellite incident shortwave radiation and photosynthetically active radiation products from multiple satellite data. **Remote Sensing of Environment**, v. 152, p. 318-332, 2014. [doi](#)
- ZHANG, X.; WANG, D.; LIU, Q.; YAO, Y.; JIA, K.; *et al.* An operational approach for generating the global land surface downward shortwave radiation product from MODIS Data. **IEEE Transactions on Geoscience and Remote Sensing**, v. 57, n. 7, p. 4636-4650, 2019. [doi](#)
- ZHANG, X.; LU, N.; JIANG, H.; YAO, L. Evaluation of reanalysis surface incident solar radiation data in China. **Scientific Reports**, v. 10, n. 1, p. 3494, 2020. [doi](#)
- ZHAO, X.; LIANG, S.; LIU, S.; YUAN, W.; XIAO, Z.; *et al.* The global land surface satellite (GLASS) remote sensing data processing system and products. **Remote Sensing**, v. 5, n. 5, p. 2436-2450, 2013. [doi](#)
- ZILLI, M.T.; CARVALHO, L.M.V.; LIEBMANN, B.; DIAS, M.A. A comprehensive analysis of trends in extreme precipitation over southeastern coast of Brazil. **International Journal of Climatology**, v. 37, n. 5, p. 2269-2279, 2017. [doi](#)
- ZULUAGA, C.F.; AVILA-DIAZ, A.; JUSTINO, F.B.; WILSON, A.B. Climatology and trends of downward shortwave radiation over Brazil. **Atmospheric Research**, vol. 250, p. 105347, 2021. [doi](#)

